Terahertz-induced population transfer between exciton complexes in monolayer WSe_2

Marzia Cuccu*,[1] Tommaso Venanzi*,[2] Edith Wietek,[1] Xiaoxiao Sun,[3] Raul Perea-Causin,[4] Takashi Taniguchi,[5] Kenji Watanabe,[6] Ermin Malic,[7] Manfred Helm,[3,8] Stephan Winnerl,[3] and Alexey Chernikov[1,*]

[1] *Institute of Applied Physics and Würzburg-Dresden Cluster of Excellence ct.qmat, TUD Dresden University of Technology, Dresden, Germany*
[2] *Center for Life Nanoscience, Istituto Italiano di Tecnologia, Rome, Italy*
[3] *Institute of Ion Beam Physics and Materials Research, Helmholtz-Zentrum Dresden-Rossendorf, Dresden, Germany*
[4] *Department of Physics, Stockholm University, Stockholm, Sweden*
[5] *Research Center for Materials Nanoarchitectonics, National Institute for Materials Science, Tsukuba, Japan*
[6] *Research Center for Electronic and Optical Materials, National Institute for Materials Science, Tsukuba, Japan*
[7] *Department of Physics, Philipps-Universität Marburg, Marburg, Germany*
[8] *Institute of Applied Physics, TUD Dresden University of Technology, Dresden, Germany*

Two-dimensional van der Waals semiconductors feature a variety of stable Coulomb-bound electron-hole complexes, which determine the optical response of the materials and serve as primary carriers of energy and spin-valley encoded information. Importantly, transitions between different excitonic states are found in the terahertz spectral range, motivating the use of strong THz radiation for their manipulation on ultrafast timescales. In this work, we apply this technique to efficiently transfer populations within the manifold of excitonic complexes in monolayer WSe_2, combining pulsed optical injection with a perturbation induced by a THz free-electron laser source. Monitoring time-resolved photoluminescence we show conversion between different Coulomb-bound species across biexcitonic and excitonic regimes. Depending on the lattice temperature, these processes involve both short-lived bright and long-lived dark states. Combining experimental findings with theory support, we outline possible dissociation and formation pathways of charged excitons and biexcitons induced by the THz radiation. Finally, we demonstrate the access to formation dynamics of charged biexcitons under controlled conditions of thermalized populations of their constituents, avoiding complications of excess energies that otherwise occur after non-resonant optical excitation.

Keywords: excitons, trions, biexcitons, terahertz, two-dimensional materials, ultrafast microscopy

I. INTRODUCTION

Low-dimensional semiconductors, such as monolayer transition-metal dichalcogenides (TMDCs), feature a variety of excitonic complexes with large binding energies that form due to strong Coulomb interactions [1, 2]. These include neutral excitons, trions [3–5] and Fermi polarons [6–9], neutral and charged biexcitons [10–14] as well as increasingly exotic states [15] up to the Mott transition [16, 17]. Excitonic complexes dominate both the optical properties of these materials and serve as primary carriers for energy and spin-valley-encoded information. Consequently, it became important to find effective means for their manipulation and tuning of their properties. A variety of successful approaches have been employed, which make use of external electric [18], magnetic [19], optical [20], and strain [21, 22] fields, changes in the dielectric environment [23] and chemical functionalization [24].

In this context, a particular challenge is to trigger conversion of one type of the excitonic species into another on ultrafast time-scales, especially from equilibrated populations of low-energy states. A useful approach, demonstrated for conceptually similar quantum well systems, is the employment of low-frequency radiation following the injection of excitons using optical pulses. Due to comparatively low binding energies of the excitonic complexes of a few meV in these systems, this was achieved using either strong microwave radiation [25–27] or frequencies on the order of a THz [28–30]. The underlying mechanisms involved impact ionization, multi-photon processes or coupling to the intra-excitonic transitions. For TMDCs, similar to bulk CuO_2 [31], the relevant energy scales are on the order of a few 10's up to 100's of meV instead. Therefore, many-THz photon energies provide access to the properties of excitonic states and their manipulation in atomically-thin materials [32–36].

Consequently, radiation in this range can be used to induce transfer between different excitonic species. As a proof of concept, we have demonstrated how a combination of optical injection with strong THz excitation by a free-electron laser can rapidly convert excitons dressed by free electrons into neutral excitons in monolayer $MoSe_2$ [37]. In close analogy to the light-induced ionization of molecules and atoms, this transient process involves photodetachment of an electron from the com-

* alexey.chernikov@tu-dresden.de

posite trion state tunable by an externally set delay between the optical and THz pulses. While highly promising, the general applicability of this approach for other types of TMDCs with a more complex excitonic structure involving long-lived dark states remains an open question. Similarly, it is unclear whether higher-particle states such as biexcitons could be manipulated in the same manner. The capacity to control biexcitons, in particular, is especially interesting given their importance for quantum information technologies and entanglement-based sources of photons [38, 39].

Here we apply the optical-pump/THz-push approach to WSe_2 monolayers, which host a rich excitonic structure involving dark states and higher-order excitonic complexes. After the optical injection and subsequent equilibration, a THz pulse with a set delay triggers a transient transfer of exciton populations within picoseconds. Monitoring time-resolved photoluminescence, we observe almost complete quenching of the dominant emission from charged biexcitons and n-type trions. This is accompanied by a transient brightening of neutral biexcitons and bright exciton states followed by subsequent reformation of charged biexcitons within a few up to tens of ps. Supported by theoretical considerations extending the description of the exciton-trion scenario to biexcitonic complexes, we discuss possible pathways and demonstrate the applicability of the approach over a broad temperature range up to 100 K. In this manner, we also gain access to the temperature dependent formation time of the charged biexcitons, avoiding the complications of substantial excess energies after more typical non-resonant optical injection conditions.

II. EXPERIMENTAL DETAILS

The investigated sample was a mechanically exfoliated WSe_2 monolayer encapsulated in hBN to reduce disorder [40, 41] and deposited on a diamond substrate using visco-elastic transfer [42]. The transparency of diamond to THz radiation prevents additional heating of the structure from the residual THz absorption. The initial optical characterization of the monolayer was performed with the sample held in a microscopy-cryostat at the temperature 5 K and using a continuous-wave laser with a photon energy of 2.3 eV for excitation. The laser was focused to a spot of 1 μm diameter by a 60x objective. For the hyperspatial mapping the power density was set to 74 W/cm^2, corresponding to an estimated steady-state electron-hole pair density on the order of 10^{10} cm^{-2}. The step size was 1 μm in both x- and y-directions. The resulting photoluminescence (PL) signals were recorded with a CCD after passing through an imaging spectrometer. A micrograph of the sample is shown in Figure 1 (a) together with a map of the bright exciton peak energy extracted from the hyperspatial photoluminescence mapping. The observed energy shifts on the order of a few 10's of meV are typical for this type of samples. They are attributed to the roughness of the diamond leading to mechanical strain that is inhomogeneously distributed in the monolayer. For the subsequent measurements we identified sufficiently large homogeneous regions with reasonably narrow linewidths of the exciton resonances.

The experimental configuration for the optical-pump/THz-push experiments is schematically illustrated in Fig. 1 (d). The sample was mounted on a cold-finger microscopy cryostat and cooled down to temperatures between 5 and 130 K. To create the initial population of the excitonic states, we used an optical pulse with a photon energy of 3.1 eV obtained from the second-harmonic of a picosecond Ti:sapphire laser. The laser was focused to a 2 μm spot on the sample using a 50x objective, resulting in typical fluence of several 10's of $\mu J/cm^2$. Narrow-band picosecond THz pulses (see Appendix A) generated with an infrared free-electron laser (FEL) [43] were then used as a perturbation to the system after an externally set time delay. PL emission from the sample was dispersed in an imaging spectrometer and detected in time by a streak camera. The THz pulse duration was approximately 5 to 10 ps and the nominal time-resolution of the PL detection, extracted from the scattered light of the optical pulse using the streak camera, was determined as 5 ps. The experiments were performed as a function of temperature, THz excitation power, and for several selected THz photon energies.

III. THZ-INDUCED TRANSITIONS BETWEEN EXCITONIC STATES

Typical low-temperature PL spectra of the investigated sample obtained under continuous-wave excitation are presented in Figure 1 (b). The spectrum recorded at a low power density shows the characteristic, spectrally narrow features of an hBN-encapsulated monolayer WSe_2 with small residual n-type doping [44–46]. The features include neutral excitons (X_0) and biexcitons (XX), bright trions (X−), neutral (D_0) and charged (D−) dark states and phonon sidebands (P) as well as charged biexcitons (XX−). Both neutral and charged biexcitons become more pronounced with increasing power density [10, 11, 13], as evidenced in the spectrum recorded at a higher excitation power presented in Figure 1 (b). This is reflected in the extracted ratios of neutral and charged biexcitons compared to the neutral exciton. At low power density these are $XX-/X_0 = 0.04$ and $XX/X_0 = 0.01$, increasing substantially for the spectrum at high power density, where $XX-/X_0 = 1.9$ and $XX/X_0 = 0.4$.

Corresponding streak camera image of the time- and spectrally-resolved PL is presented in Figure 1 (c). The photon energies of the peaks are plotted on a scale relative to the X_0 resonance at 1.72 eV. The emission spectrum matches the main resonances of the continuous-wave measurement aside from potential photodoping and additional broadening. The latter stems from the larger excitation area, smaller spectral resolution of the setup

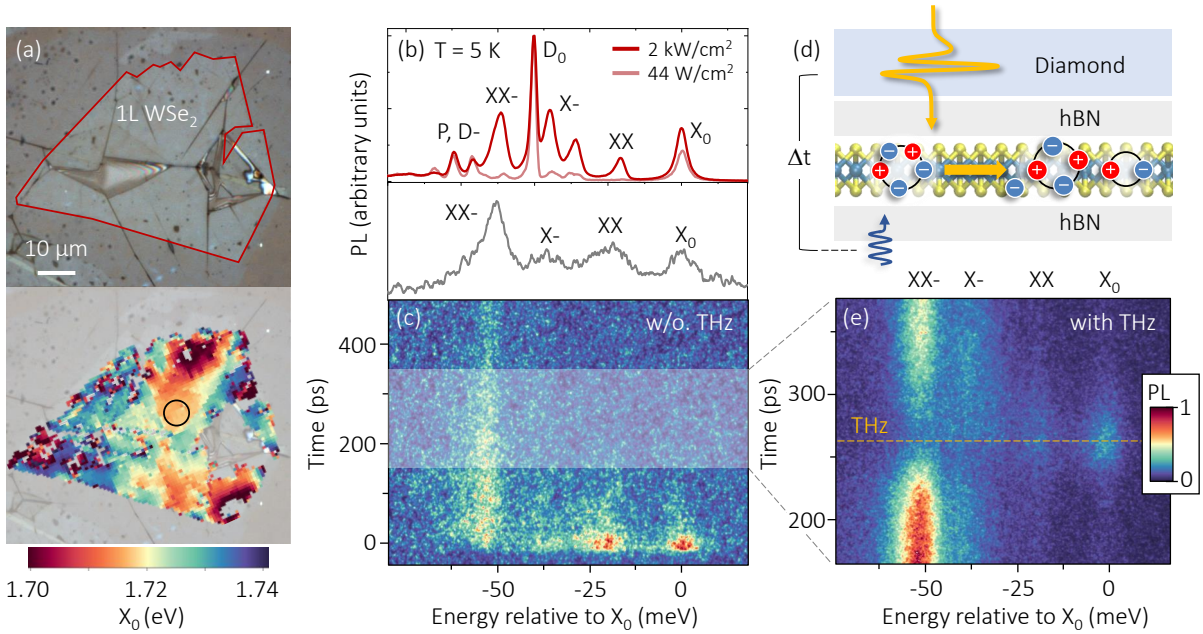

FIG. 1. (a) Top panel: optical micrograph of the sample with the highlighted WSe_2 monolayer. Bottom panel: spatial map of the bright exciton energy peak extracted from the PL spectra at 5 K under continuous wave excitation, superimposed on the optical image. The black circle marks the area where the optical-pump/THz-push measurements were performed. (b) A representative PL spectra of the WSe_2 sample under continuous wave excitation at high (2 kW/cm^2) and low (44 W/cm^2) power densities. (c) Spectrally- and time-resolved streak camera image in absence of terahertz pulse and the corresponding time-integrated PL spectrum obtained for pulsed excitation using the fluence of 28 μJ/cm^2 per pulse. The shaded white area indicates the time range studied in the subsequent measurements involving THz excitation. (d) Schematic illustration of the experimental setting for the optical-pump/THz-push experiments. Δt indicates the time delay between the optical and the THz pulses. (e) Streak camera image of the PL in the presence of a strong THz pulse, with a fluence of 30 μJ/cm^2, that arrives with a time delay of 250 ps after the optical excitation.

for time-resolved experiments and, most importantly, higher optical pump density. In particular, the fluence of the pulsed laser of 30 μJ/cm^2 corresponds to the average power density of 6 MW/cm^2, which is three orders of magnitude higher than that used for the high-power PL spectrum shown in Figure 1 (b). This leads to a further enhancement of the PL intensity ratio of XX− and XX compared to X_0). The spectrum in Fig.1 (b) (bottom), yields PL ratios of XX−/X_0 = 3.2 and XX/X_0 = 0.8, both of which are significantly higher than the corresponding values extracted from the spectra under continuous-wave excitation. The absence of the D_0 feature is attributed to both high fluence with the dominant XX- emission and the limited observation time window in the spectrally- and time-resolved measurements.

After the optical excitation at t = 0 ps, the bright states X_0 and X− (representing the trion doublet) decay within a few 10's of picoseconds, while charged biexciton, that is composed of a bright and a dark state, decays much slower over a few 100's of picoseconds. For the experiments involving THz excitation, we thus focus on this later time range, as indicated by the shaded region in the bottom panel of Fig. 1 (c). This enables us to investigate the case of thermalized excitonic populations [47, 48] when only the long lived XX− state and a residual trace of bright trions are visible. We also note, that, while the image presented in Figure 1 (c) was recorded as a general overview, the overall acquisition time was increased substantially for all subsequent measurements to ensure high signal-to-noise ratios.

When the THz pulse arrives, at t_{THz} = 250 ps after the optical excitation, the emission dynamics changes substantially, as shown in Figure 1 (e). For this measurement, the photon energy and fluence of the THz beam were set to 14 meV and 30 μJ/cm^2, respectively. The magnitude of the changes is overall similar to the previously studied case of the $MoSe_2$ monolayer [37], albeit both the time delays are substantially longer and the origin of the emission involves biexcitons in the present case. Here, the THz radiation causes a strong quenching of the charged biexciton and residual trion populations and induces a brightening of both neutral exciton and biexciton states. The quenching occurs on the same timescale for charged biexcitons and trions within the time-resolution of the setup (see Appendix B). The impact of the THz pulse resembles an effective reset to the initial conditions of the system at time t = 0, corresponding to the excitation by the optical pulse. This effect is evident in the broadening of the trion emission, potentially related to a higher temperature of the electronic distribution [36] and

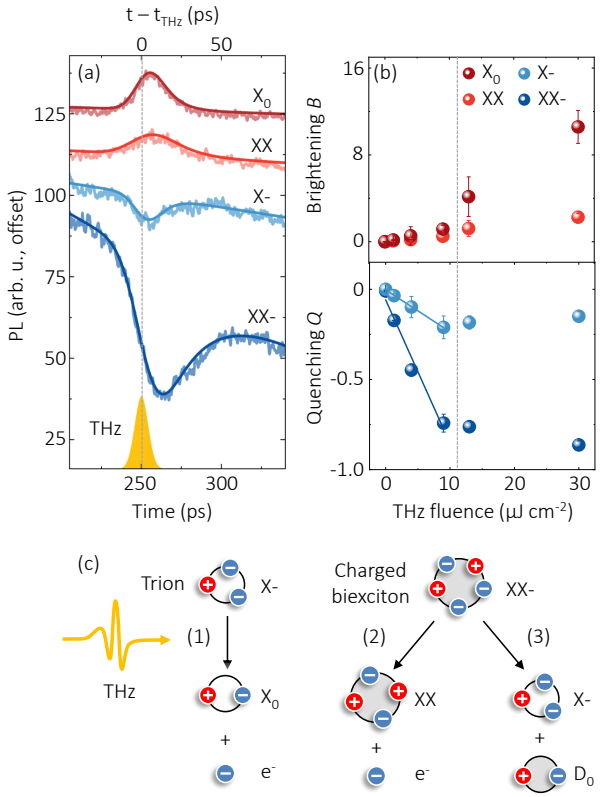

FIG. 2. (a) PL transients extracted at the energies of the excitonic resonances in the time window of the THz pulse arrival presented together with the corresponding fit curves. The characteristic time constants for the THz pulse arrival are of similar values for all fit curves within the temporal resolution of 5 ps. Maximal duration of the THz pulse is added for comparison. The fluence of the THz pulse 30 μJ/cm^2 (b) Top panel: brightening factor B of the bright exciton X_0 and neutral biexciton XX as a function of the THz fluence. Bottom panel: quenching factor Q of the negative trion X− and the charged biexciton XX−; the gray dashed line separates the linear regime from the saturation regime. (c) Schematic illustration of the possible THz-induced dissociation pathways of the trions and charged biexciton. Gray shading indicates contributions of the spin-dark states.

its impact on the trion lineshape via recoil effect [49]. In addition, the increase of the intensity at the high energy side of the trion could similarly stem from the transient redistribution of the PL intensity within the spin-split trion doublet [50] (see Appendix C). Here, the higher energy trion initially exhibits higher PL intensity that shifts towards the lower energy trion at later times [51]. We thus speculate that the arrival of the THz pulse returns the distribution of the PL within the trion-doublet to the conditions resembling those immediately after the optical excitation.

Most importantly, however, the simultaneous change in dynamics demonstrates an effective population transfer between charged and neutral excitonic complexes, illustrated by the corresponding PL transients presented in Figure 2 (a). These are obtained by integrating the PL signal over the spectral region of interest of each peak, after the background subtraction of the streak camera image. We also add the time scale $t - t_{THz}$, relative to the arrival of the THz pulse, and use it for the rest of the presented data. Following the THz-induced redistribution of the PL intensity, the initial PL counts prior to the THz pulse arrival recover within 10's of ps. We also note that the initial changes of the dynamics occur on the same time-scale during THz-pulse arrival. Slight differences in the positions of the minima and maxima are attributed to the interplay of depopulation and population dynamics, as discussed in more detail below, as well as differences in the reformation times that are either fast or slow, depending on the given state.

For the analysis of the THz-induced dynamics we note, that the full picture of interacting charged and neutral exciton and biexciton states is a very complex problem and is currently not accessible in a unified, microscopic framework. We thus use both qualitative comparison with the generic picture of a charged-to-neutral transfer scenario further below and phenomenological fitting of the experimental data. In particular, the transients of the excitonic peaks are fitted with a single exponential function multiplied by a Heaviside function, convoluted with a Gaussian to account for the limited time resolution of the experiment given by the streak camera resolution and the pulse lengths. The resulting fitting function is the following:

$$PL(t) = \frac{\gamma}{N} H(t - t_0)\, e^{-(t - t_{THz})/\tau} + a\,t + b,$$

where the parameter γ is the quenching (if negative) or brightening (if positive) factor, N is a normalization factor to the intensity prior to the THz pulse arrival at t_{THz}, τ is the time characteristic constant of the recovery. $H(t - t_0)$ indicates the modified Heaviside function $erfc\big(-(t - t_0)/\sqrt{2}\sigma + \sigma/\sqrt{2}\tau\big)$, where σ is the standard deviation of the Gaussian function. The linear term $(a\,t + b)$ approximates the PL emission dynamics in this very short time-window compared to the overall long decay time of the signal.

Using this fit function we extract the brightening B of the X_0 and XX states and the quenching Q of the X− and XX− states. The extracted quenching and brightening factors are subsequently normalized with respect to the PL intensity of the corresponding populations at time t_{THz} in the absence of THz radiation, enabling a quantitative analysis of the impact of the FEL on each excitonic population. The resulting values are shown in Figure 2 (b) as a function of THz fluence. The initial linear dependence of both quenching and brightening factors indicates a predominant one-photon origin of the underlying processes. At higher fluences, it is likely that the finite doping density in the material contributes to the saturation of the quenching. We note, however, that due to the potential competition of the THz-induced dissociation and filling dynamics of the trion state in partic-

ular, quantitative assessment of the saturation behavior is likely to be more complex. The brightening of the XX also saturates, while the intensity of the X_0 state continues to increase at higher powers. While this difference stems from the data point for the highest THz fluence, one could in principle consider THz-induced dissociation of the bright trions to serve as an additional pathway to create neutral excitons.

In general, there are several possible dissociation channels for the initial populations of trion and charged biexciton states at the arrival of the THz pulse, as schematically illustrated in Fig. 2 (c). Upon THz photon absorption, a trion separates into a bright exciton and a free electron ($e-$):

$$X- \rightarrow X_0 + e- . \tag{1}$$

For the charged biexciton, being a five particle state, in analogy to the negative ion of the hydrogen molecule H_2^- [52, 53], two pathways are in principle possible. It can separate into a neutral biexciton and a free electron

$$XX- \rightarrow XX + e-, \tag{2}$$

or, alternatively, dissociate into a (dark/bright) exciton and a (bright/dark) trion, considering the typical composition of the charged biexciton binding an electron, a bright and a dark exciton states [54]:

$$XX- \rightarrow D_0 + X- . \tag{3}$$

The process of trion photodetachment (1) accounts for the quenching of the trion population and should also serve as the primary source for the observed brightening of the neutral exciton. We note, however, that this process may not be highly efficient in absolute terms as the energy of THz pulse of 14 meV is below the trion binding energies in the range of 30 meV [50]. The second process of charged biexciton dissociation, (2), then acts as a main source for the THz-induced population of neutral biexcitons. Similar to X_0, the low intensity of the brightening is attributed to the different THz photon and charged biexciton binding energies. The latter is similar to the trion binding energy of about 30 meV as extracted from the energy separation between the XX− and the XX states. Finally, the dissociation process (3), with a binding energy in the range of 20 meV, contributes to the strong decrease of the XX− states while simultaneously increasing the trion population. This should account for the bleaching of the trion being less pronounced compared to that of the charged biexciton. Moreover, channel (3) may also produce bright excitons either directly or from the dissociation of trions.

In addition, higher-order processes, cannot be fully excluded as a contribution to the brightening of the neutral exciton, especially at elevated THz fluence. We also note that similar observations are obtained for the lower (9 meV) and higher (35 meV) photon energies of the THz pulse (see Appendix D). This may further indicate the additional role of higher-order processes, while precluding reliable statements regarding the resonance behavior due to the coarse energy intervals between these measurements.

In principle, the two dissociation processes of the charged biexciton, (2) and (3), can be conceptually considered as the biexcitonic versions of the trion photodetachment, (1). Thus, the model used to describe the latter [37] can be adjusted by changing the effective masses of its constituents. In that case biexcitons and trions are taking the role of excitons and electrons, respectively, in this simplified description (see Appendix E). Then, the matrix element for the THz-induced dissociation depends only on the Bohr radius and the reduced mass of the composite exciton states involved. Comparing the case of the trions and charged biexcitons, the reduced masses are $\mu_{X-} = m_X m_e/(m_X + m_e)$ and $\mu_{XX-} = 2m_X m_e/(2m_X + m_e)$, respectively. Assuming $m_e = m_h$, that reasonably applies for WSe_2, the resulting differences in the reduced masses are rather small with $\mu_{X-} = 2/3m_e$ and $\mu_{XX-} = 4/5m_e$. Thus, despite much heavier total mass, the reduced mass of the charged biexciton is only 20 % higher than that of the trion, rendering the processes (1) and (2) very similar. For the dissociation pathway (3) into an exciton and a trion the difference is factor of two, rendering it even more efficient for sufficiently high THz photon energies compared to (1) (see Appendix E).

We note that we addressed the dissociation of charged excitonic particles in terms of photon energy rather than THz-field-driven ionization. This choice is qualitatively motivated by estimating the THz electric field strength relative to the relevant binding energies. The maximum electric field in air is about 60 kV/cm at 30 μJ/cm^2 an 87 μm, corresponding to a ponderomotive energy of about $U_p = \frac{e^2 E_{THz}^2}{4m^* \omega_{THz}^2} = 3$ meV. Considering the exciton binding energy of a about $I_p = 300$ meV, the Keldysh parameter is $\sqrt{\frac{I_p}{2U_p}} \sim 10$ [55]. This condition is far from the field-regime and supports the use of a photon-energy-based description.

IV. TEMPERATURE-DEPENDENT DYNAMICS

The observed interplay between different excitonic complexes in WSe_2 triggered by THz radiation motivates temperature-dependent measurements to change the population of the initial states. Streak camera images at selected temperatures are presented in Figure 3 (a) together with the extracted transients at individual resonances and corresponding fits shown in (b). The complete data set is presented in Appendix F. The PL decays of the four resonances are obtained by summing over the energy regions of Figure 3 (a), each centered at the energy of the corresponding excitonic state. Overall, it shows that THz-induced population transfer in WSe_2 monolayers is a robust effect with respect to temperature,

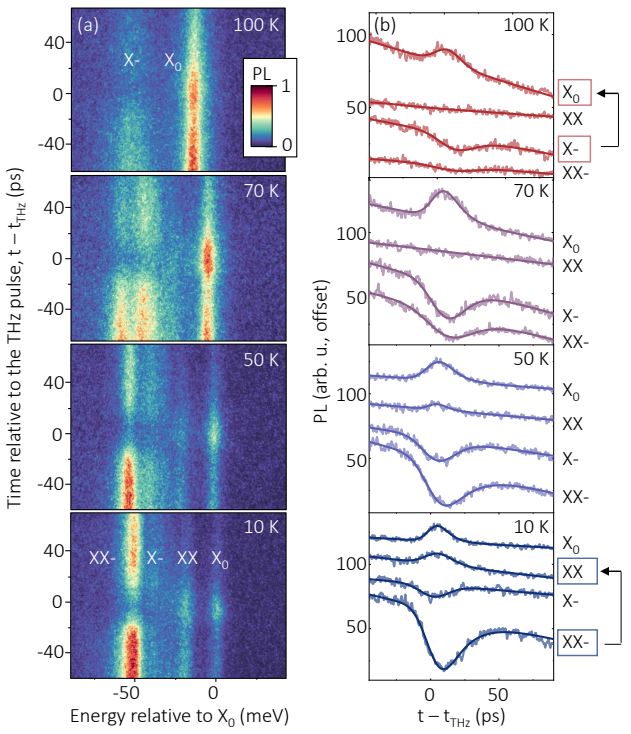

FIG. 3. (a) Streak camera images of the spectrally- and time-dependent PL for different temperatures in the time range of the THz pulse arrival. The energy scale on the x-axis is relative to the X_0 resonance at 5 K. (b) Transients extracted at the energies of charged biexciton, negative trion, neutral biexciton and bright exciton together with the fit curves. The arrows indicate dominant THz-induced dissociation processes at 5 and 100 K. The THz pulse fluence used for the temperature dependent measurements is 20 μJ/cm^2

observed up to 130 K. Two distinct regimes are identified: at low temperatures the predominant process is the dissociation of the charged biexcitons, while, at higher temperatures only the interplay between bright trions and excitons remains.

Based on these observations, all three dissociation channels outlined above are active up to 50 K. Around 50 K, a transition regime begins where the charged biexcitons become increasingly less populated due to the elevated temperature and their emission intensity gradually decreases [10, 11]. This interplay is particularly evident at 70 K. At this temperature, also the brightening of the neutral biexcitons is completely suppressed, as further illustrated in the corresponding transient presented in Fig. 3 (b). Simultaneously, the gradual depopulation of charged biexcitons leads to a decrease of dissociation channel 3, resulting in reduced trion formation. This, in turn, induces a more pronounced quenching of the trion population. For even higher temperatures of 100 K and above, the only states that remain in the system are the bright excitons X_0 and trions X−. The quenching dynamics extracted at the spectral position of the XX− resonance can thus stem from the shoulder of the broadened X− peak in the 100 K data. Consequently, the process triggered by the arrival of the THz radiation is the one associated with (1). This result closely resembles the behavior of $MoSe_2$ monolayers at low temperature [56] further supporting the direct dissociation of trions into bright excitons and free electrons, as discussed in Section III.

For the analysis, fits of the transients provide quenching and brightening factors of the four states for increasing temperature, as presented in Figs. 4 (a) and (b) for bright excitons and charged biexcitons, respectively. These allow for the quantitative assessment of the two temperature-dependent regimes, as shown in Figure 4 (c). Notably, a crossover of the quenching factors of XX− and X− is observed around 70 K, originating in the thermal dissociation of the biexciton states, as discussed above. Specifically, the quenching factor of XX−, which dominates at low temperatures, strongly decreases due to the gradual vanishing of the dissociation channels 2 and 3 caused by the thermal instability of the charged biexciton. In principle, one can also consider the heating of the excitonic complexes by the THz radiation, leading to decreased recombination rate and thus quenching. If the lattice temperature is already high, the additional heating should be less pronounced. Moreover, increasingly faster reformation dynamics, as shown in panel (d), approaching the time-scales of the THz-pulse length should render the quenching less pronounced due to simultaneous refilling. In contrast, the initially higher population of the trions with increasing temperature attributed to the thermal dissociation of biexcitons also leads to an increase in the quenching factor of X−. At the same time, the gradual suppression of the brightening factor of X_0 reflects the strong increase of the bright exciton population, which becomes dominant at higher temperatures. The brightening of the neutral biexciton, XX, slightly decreases and vanishes completely at temperatures around 50 K.

Particularly interesting is the extracted time τ_{form} for the re-formation of the charged biexciton as a function of temperature, shown in Figure 4 (d). The values are extracted from the fits to the rising profile of the XX− after the arrival of the THz pulse and are substantially larger than the temporal resolution of the measurements. Importantly, here charged biexcitons are created with a low kinetic energy due to the quasi-resonant condition with the THz radiation. Therefore, we are able to analyze the re-formation times in a pristine manner, avoiding any cooling and relaxation processes that otherwise would occur after optical excitation. The overall behavior and the obtained time scales resemble the characteristics of trion and free carrier cooling times [49, 56] as well as relaxation timescales typically found for excitonic complexes[57, 58]. These values are thus indicative of charged biexciton formation mediated by phonon scattering. As the temperature increases, the phonon-assisted processes become more likely due to the occupation of

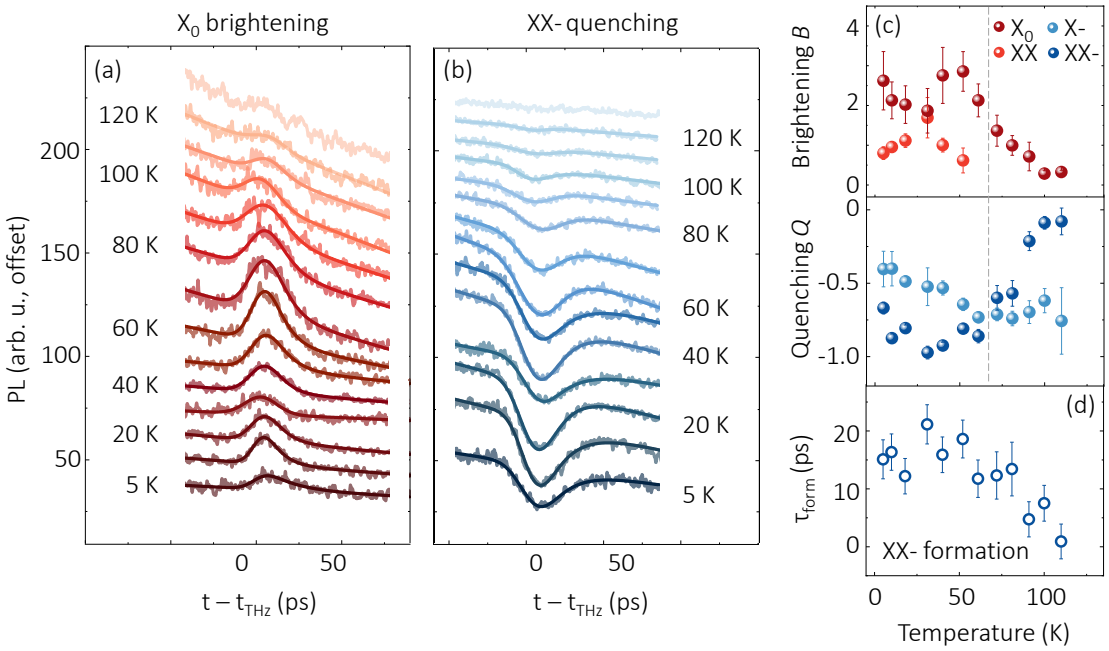

FIG. 4. Transients of the bright exciton (a) and the charged biexciton (b) PL for increasing temperature with corresponding fit to the curves. (c) Top: brightening factor B of bright exciton (dark red) and neutral biexciton (red) as a function of temperature at the time of arrival of the THz pulse. Bottom: quenching factor Q of negative trion (light blue) and charged biexciton (blue) as a function of temperature at the same time as for the upper panel. Brightening and quenching factors are normalized with respect to the PL of the peak in the absence of the THz pulse. The gray dashed line indicates two regimes: the left one, in which the population is dominated by dark states, and the right one, in which only bright states are left in the system. (d) Re-formation time of the charged biexciton extracted from the fits in (b) as a function of temperature.

both optical and acoustic zone-edge modes [59]. In addition to phonons, however, the re-formation of charged biexcitons under the emission of photons could also be in principle possible. This would correspond to the reverse pathways of (2) and (3) mechanisms, involving either a capture of an electron by a neutral biexciton or the binding of an exciton to a trion, with the consequent emission of a THz photon.

V. CONCLUSION

We have demonstrated transient population transfer on picosecond time-scales between charged and neutral excitonic complexes via THz absorption in WSe_2 monolayers. At highest THz fluences we report almost complete depletion of the charged biexciton and trion populations leading to the emergence of the biexciton and exciton luminescence. We discuss possible dissociation channels and demonstrate the phenomenon for a broad range of temperatures, from 4 up to 130 K. Two characteristic regimes are observed, dominated by the THz radiation coupling primarily to either charged biexcitons and trions as a direct consequence of the changes in thermal populations. In this manner, we also gain access to the temperature-dependent formation time of the charged biexciton during the relaxation of the excitonic system. Altogether, these findings show the general applicability of using THz radiation to switch between populations of different excitonic states, including exciton molecules in atomically-thin semiconductors. Both the manipulation of the exciton complexes on ultrafast time-scales as well as the additional insights into the quasiparticle formation dynamics are expected be useful for a wide range of excitonic materials. One can also consider the application of the approach to excitons coupled to correlated electronic states as well as consider its use for non-linear optics and photonics merging optical and THz excitations in ultrathin crystals.

VI. ACKNOWLEDGMENTS

We thank M. M. Glazov and L. Baldassarre for helpful discussions. Financial support by the DFG via Emmy Noether Initiative (CH 1672/1, project ID 287022282, A.C.), SFB 1277 (project B05, project ID: 314695032, A.C.) and SFB1083 (project B09, project ID 223848855, E.M.), DFG project Propagation dynamics of exciton electron complexes in atomically-thin semiconductors (project ID 542873285, E.M., A.C.), the Würzburg-Dresden Cluster of Excellence on Complexity and Topology in Quantum Matter (ct.qmat) (EXC 2147, project ID 390858490, A.C.) is gratefully acknowledged.

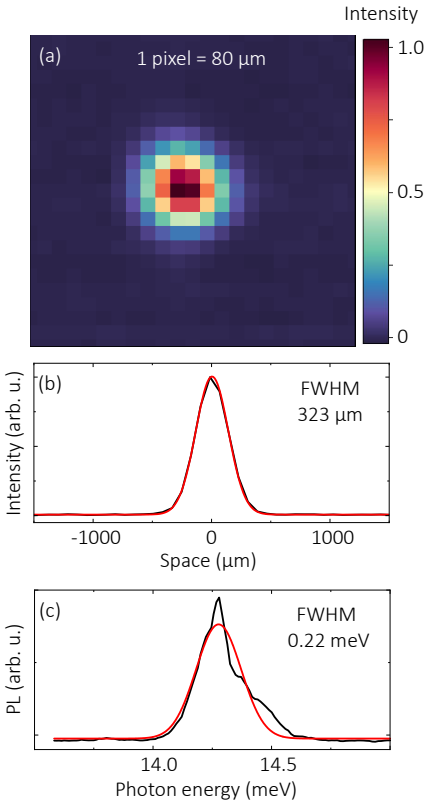

FIG. 5. (a) Pyroelectric camera image of a representative FEL beam with the photon energy of 14 meV (3.4 THz). The size of one pixel corresponds to 80 um. (b) Extracted profile from the image in (a) along with a Gaussian fit to the data. From the fit, a full-width-at-half-maximum of 323 μm was obtained at the sample position for an FEL beam at energy of 14 meV. (c) Normalized spectrum of the THz pulse at photon energy of 14 meV. The extracted full-width-at-half-maximum of 0.22 meV was extracted from the Gaussian fit in red.

Parts of this research were carried out at ELBE at the Helmholtz-Zentrum Dresden-Rossendorf e.V., a member of the Helmholtz Association. We thank A. Wagner and the ELBE team for support. A.C. acknowledges funding from ERC through CoG CoulENGINE (GA number 101001764). K.W. and T.T. acknowledge support from the JSPS KAKENHI (grant numbers 20H00354, 21H05233 and 23H02052) and World Premier International Research Center Initiative (WPI), MEXT, Japan.

M. C. and T. V. contributed equally to this manuscript.

Appendix A: THz spectrum and spot size

To capture the FEL beam size at the sample position, a pyroelectric infrared camera was used. The dimension of the beam varies within the range of hundreds of μm depending on the energy of the THz pulse. Figure 5 (a) shows an exemplary image of the FEL spot size at an energy of 14 meV, which corresponds to the energy used for the results presented in the main manuscript. The corresponding intensity profile, along with a Gaussian fit to the data, is shown in Figure 5 (b), yielding a full-width-at-half-maximum of 323 μm at the sample position. For reference, a representative normalized spectrum of the THz source centered at 14 meV is presented in Figure 5 (c), along with the Gaussian fit and the extracted full-width-at-half-maximum of 0.22 meV, corresponding to a pulse duration of approximately 5 ps.

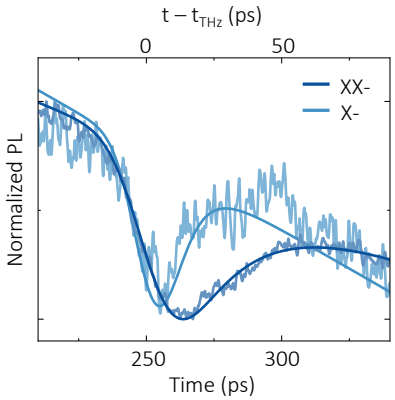

FIG. 6. Normalized (in intensity) transients of the charged biexciton (XX-) and trion (X-) emission corresponding to the data from Figure 1 (e) of the main text. The data is shown together with phenomenological fit curves modeling both rise and decay with exponentials.

Appendix B: Trion and charged biexciton transients

With the arrival of the THz radiation, both charged biexciton and trion populations undergo strong quenching on similar timescales, as shown in Figure 6. Here, the time zero, defined as the half-time of the initial THz-induced intensity decrease, is extracted from the fits to the data using the function described in the main text. The extracted values are the same for both excitonic populations within the experimental uncertainty of several picoseconds. This indicates that the initial quenching occurs simultaneously, but due to the faster reformation dynamics of the trions, their minimum appears at earlier times compared to that of the charged biexciton transient.

Appendix C: PL spectra before and after the THz pulse

From the streak camera image in Figure 1 (e), the PL spectra are extracted at the times just before and after the arrival of the THz pulse, as shown in Figure 7. This direct comparison reveals an additional broadening of the

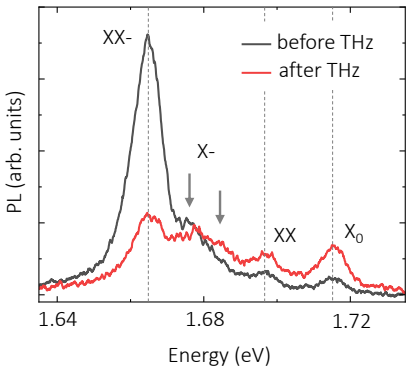

FIG. 7. PL spectra before (black) and after (red) the arrival of the THz pulse, as extracted from the streak camera image shown in Figure 1 (e) of the main text. The arrows indicate the two spin-split trions.

trion (X-) emission by approximately 10 meV in the spectrum extracted after the arrival of the THz pulse, along with the appearance of a shoulder on the higher-energy side. The broadening could be associated with the increase of the trion PL flank related to the increase of the electronic temperature and recoil effect [36, 49]. A probable cause to the increased PL at the higher-energy flank is the consequence of the trion dissociation and the subsequent reformation. Specifically, the trion in WSe_2 is split into a doublet peak due to exchange interaction [50]. After optical excitation, the higher-energy trion usually exhibits stronger PL, followed by the subsequent redistribution into the lower-energy trion [51]. Here, the THz pulse acts as an effective reset of the initial conditions of the system at the time of the optical excitation, leading to the reappearance of the higher-energy trion, observed as a shoulder in the red spectrum in Figure 7.

Appendix D: Dissociation dynamics for different THz photon energies

The presented spectrally- and time-resolved measurements were repeated at 5 K also for two additional THz photon energies, one below (9 meV) and one above (35 meV) the value presented in the main text. In both cases, the results were similar to those obtained for the 14 meV photon energy. Specifically, with the arrival of the THz pulse, we observe a transient quenching of the chanrged biexciton and negative trion populations, accompanied by a brightening of the bright exciton and neutral biexciton populations. Brightening B of bright exciton and neutral biexciton as well as quenching Q of negative trion and charged biexciton are extracted from the fits to the transient profiles and normalized as described in the main text. The obtained values are shown per unit fluence in Figure 8 as a function of the THz photon energy. The data does not show any strong

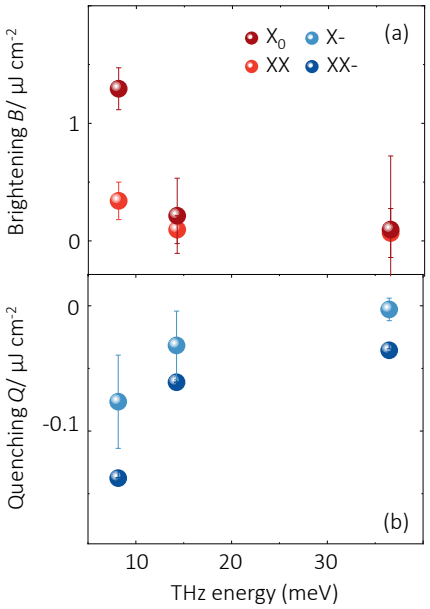

FIG. 8. (a) Brightening factor B per unit fluence of bright exciton and neutral biexciton as a function of the THz photon energy at the time of arrival of the THz pulse. (b) Quenching factor Q per unit fluence of negative trion and charged biexciton as a function of the THz photon energy at the same time as for (a).

dependence on the THz energy, indicating that the efficiency of the transfer processes between neutral and charged states remains constant in the studied range. This behavior could indicate that additional contribution of higher-order processes may be involved in the THz-induced transfer processes. Nonetheless, due to the coarse energy scan between the measurements, the data does not allow to draw definitive conclusions regarding specific resonance conditions.

Appendix E: Adaptation of the trion dissociation model to charged biexcitons

In Ref. [37] we modeled the conversion from charged into neutral excitons induced by a THz field with the matrix element $\mathbf{d_k} = e_0 \int d^2\mathbf{r}\, \psi^*(\mathbf{r})\, \mathbf{r}\, \phi_{\mathbf{k}}(\mathbf{r})$. The latter describes the transition of an electron bound to the exciton into a free electron with relative momentum $\mathbf{k}$. The bound and unbound states correspond to charged and neutral excitons and are phenomenologically modeled by the wave functions $\psi(\boldsymbol{r}) = \sqrt{2/\pi a^2}\exp(-|\mathbf{r}|/a)$ and $\phi_{\mathbf{k}}(\mathbf{r}) = \exp(i\,\mathbf{k}\cdot\mathbf{r})/\sqrt{A}$, respectively, with the Bohr radius a and the system area A. Here, we extend this model to account for the conversion from charged biexcitons into neutral biexcitons. In the same spirit, an electron bound to a biexciton can be described by the wave function $\psi(\mathbf{r})$, and the same approach can be employed.

The conversion rate reads

$$\gamma_i(\hbar\omega) = \frac{2\pi}{\hbar}\sum_{\mathbf{k}} |\mathbf{E}\cdot\mathbf{d}_{\mathbf{k}}|^2 \delta\left(\hbar\omega - \Delta_i - \frac{\hbar^2\mathbf{k}^2}{2\mu_i}\right), \quad \text{(E1)}$$

where i denotes either charged excitons ($i = \mathrm{X}^-$) or charged biexcitons ($i = \mathrm{XX}^-$). Here, we have introduced the charged exciton and biexciton reduced masses $\mu_{\mathrm{X}^-} = m_{\mathrm{X}}m_{\mathrm{e}}/(m_{\mathrm{X}}+m_{\mathrm{e}})$, $\mu_{\mathrm{XX}^-} = m_{\mathrm{XX}}m_{\mathrm{e}}/(m_{\mathrm{XX}}+m_{\mathrm{e}})$, the binding energy Δ_i, and the THz photon energy $\hbar\omega$. Using the analytical expression for the matrix element, $\mathbf{d}_{\mathbf{k}} \propto a^2(a\mathbf{k})/[1+(a\mathbf{k})^2]^{5/2}$, the conversion rate reads

$$\gamma_i(\varepsilon) = \frac{18\pi}{\hbar}|e_0\mathbf{E}|^2 a_i^2 \xi_i \frac{\xi_i\varepsilon}{[1+\xi_i\varepsilon]^5}\Theta(\varepsilon), \quad \text{(E2)}$$

with $\varepsilon = \hbar\omega - \Delta_i$ and $\xi_i = 2\mu_i a_i^2/\hbar^2$. This approach can also be used to describe the conversion from a charged biexciton into a neutral and a charged exciton by having the charged exciton take the role of the electron above, i.e. considering the reduced mass $\mu'_{\mathrm{XX}^-} = m_{\mathrm{X}}m_{\mathrm{X}^-}/(m_{\mathrm{X}}+m_{\mathrm{X}^-})$.

Appendix F: Temperature dependent measurements: complete data set

Here, we present the complete data set of the temperature dependent measurements. Streak camera images of the spectrally- and time-resolved PL measured with temperature between 130 and 5 K are shown in Figure 9 from the top left (130 K) to the bottom right (5 K) panel. Note that, as mentioned in the main text, the energy scale is relative to the bright exciton X_0 resonance at 5 K and the time scale is relative to the time arrival of the THz pulse. The extracted transients for all temperatures, with corresponding fits, are illustrated in Figure 10 for neutral biexciton XX_0 (a) and negative trion X− (b), and in Figure 4 of the main text for bright exciton X_0 (a) and charged biexciton XX− (b). The transition between biexcitonic and excitonic regimes are clearly identified. Specifically, at 5 K all four resonances (X_0, XX, X−, XX−) are present, with the predominant THz-induced process being the dissociation of charged biexcitons, following the pathways (2) and (3) described in Section III of the main text. These two channels, together with the one related to the trion (1), coexist up to around 60 K. Above this temperature, as illustrated in the transient profiles of Figure 10 (a), the brightening of the charged biexciton is suppressed and with this also the dissociation channels (2) and (3). At the same time, neutral exciton and negative trion populations gain in intensity, dominating the dynamics at higher temperatures. Therefore, the only process activated by the THz radiation in this regime is the one related to the trion dissociation (1). Overall, the THz-induced population transfer in monolayer WSe_2 is shown to be robust with respect to temperature, persisting up to 130 K.

[1] G. Wang, A. Chernikov, M. M. Glazov, T. F. Heinz, X. Marie, T. Amand, and B. Urbaszek, Colloquium : Excitons in atomically thin transition metal dichalcogenides, Reviews of Modern Physics **90**, 021001 (2018).

[2] R. Perea-Causin, D. Erkensten, J. M. Fitzgerald, J. J. P. Thompson, R. Rosati, S. Brem, and E. Malic, Exciton optics, dynamics, and transport in atomically thin semiconductors, APL Materials **10**, 10.1063/5.0107665 (2022).

[3] K. F. Mak, K. He, C. Lee, G. H. Lee, J. Hone, T. F. Heinz, and J. Shan, Tightly bound trions in monolayer MoS_2., Nat. Mater. **12**, 207 (2013).

[4] J. S. Ross, S. Wu, H. Yu, N. J. Ghimire, A. M. Jones, G. Aivazian, J. Yan, D. G. Mandrus, D. Xiao, W. Yao, and X. Xu, Electrical control of neutral and charged excitons in a monolayer semiconductor., Nat. Commun. **4**, 1474 (2013).

[5] R. Perea-Causin, S. Brem, O. Schmidt, and E. Malic, Trion Photoluminescence and Trion Stability in Atomically Thin Semiconductors, Physical Review Letters **132**, 036903 (2024).

[6] M. Sidler, P. Back, O. Cotlet, A. Srivastava, T. Fink, M. Kroner, E. Demler, and A. Imamoglu, Fermi polaron-polaritons in charge-tunable atomically thin semiconductors, Nature Physics **13**, 255 (2017).

[7] Y.-C. Chang, S.-Y. Shiau, and M. Combescot, Crossover from trion-hole complex to exciton-polaron in n -doped two-dimensional semiconductor quantum wells, Physical Review B **98**, 235203 (2018).

[8] D. K. Efimkin, E. K. Laird, J. Levinsen, M. M. Parish, and A. H. MacDonald, Electron-exciton interactions in the exciton-polaron problem, Physical Review B **103**, 075417 (2021).

[9] M. M. Glazov, Optical properties of charged excitons in two-dimensional semiconductors, The Journal of Chemical Physics **153**, 034703 (2020), arXiv:2005.05829.

[10] Y. You, X. Zhang, T. C. Berkelbach, M. S. Hybertsen, D. R. Reichman, and T. F. Heinz, Observation of biexcitons in monolayer WSe2, Nat. Phys. **11**, 477 (2015).

[11] S.-Y. Chen, T. Goldstein, T. Taniguchi, K. Watanabe, and J. Yan, Coulomb-bound four- and five-particle intervalley states in an atomically-thin semiconductor, Nature Communications **9**, 3717 (2018).

[12] Z. Ye, L. Waldecker, E. Y. Ma, D. Rhodes, A. Antony, B. Kim, X.-X. Zhang, M. Deng, Y. Jiang, Z. Lu, D. Smirnov, K. Watanabe, T. Taniguchi, J. Hone, and T. F. Heinz, Efficient generation of neutral and charged biexcitons in encapsulated WSe2 monolayers, Nature Communications **9**, 3718 (2018).

[13] Z. Li, T. Wang, Z. Lu, C. Jin, Y. Chen, Y. Meng, Z. Lian, T. Taniguchi, K. Watanabe, S. Zhang, D. Smirnov, and S.-F. Shi, Revealing the biexciton and trion-exciton complexes in BN encapsulated WSe2, Nature Communications **9**, 3719 (2018).

[14] M. Barbone, A. R.-P. Montblanch, D. M. Kara, C. Palacios-Berraquero, A. R. Cadore, D. De Fazio, B. Pingault, E. Mostaani, H. Li, B. Chen, K. Watan-

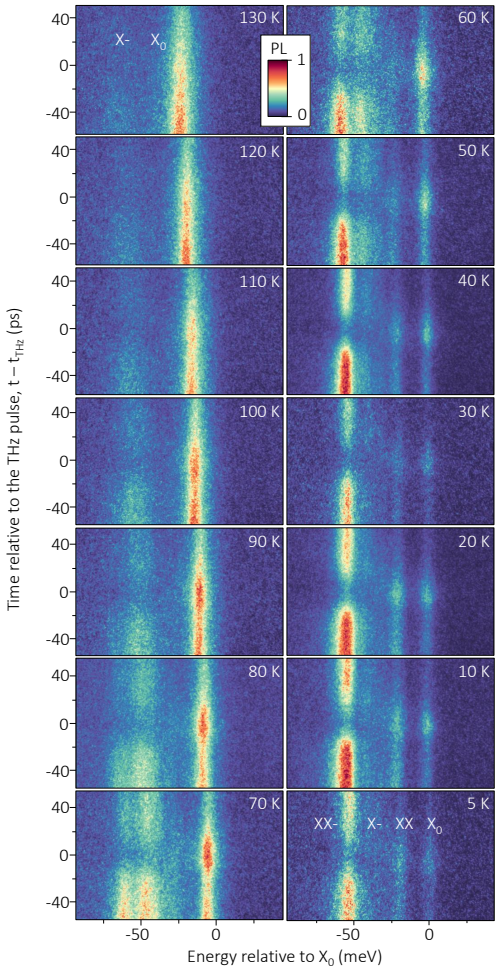

FIG. 9. Streak camera images of the spectrally and time-dependent PL for temperature between 5 and 130 K in the time range of the THz pulse arrival. The energy scale is relative to the bright exciton resonance at 5 K.

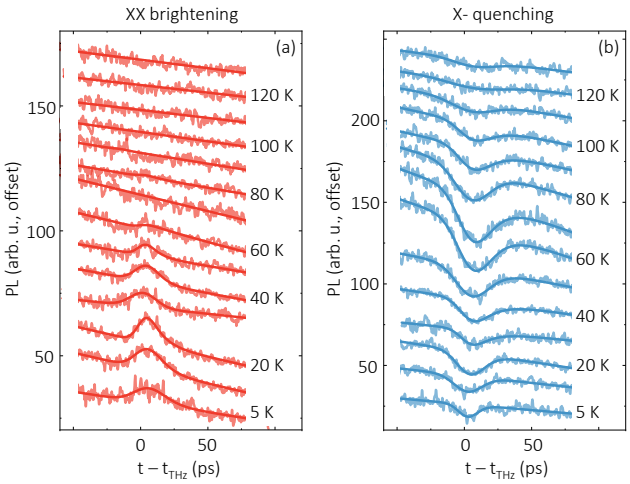

FIG. 10. Transients of the neutral biexciton (a) and the negative trion (b) PL for increasing temperature with corresponding fit to the curves.

abe, T. Taniguchi, S. Tongay, G. Wang, A. C. Ferrari, and M. Atatüre, Charge-tuneable biexciton complexes in monolayer WSe2, Nature Communications **9**, 3721 (2018).

[15] D. Van Tuan, S.-F. Shi, X. Xu, S. A. Crooker, and H. Dery, Hexcitons and oxcitons in monolayer WSe_2, arXiv (2022), 2202.08375.

[16] A. Chernikov, C. Ruppert, H. M. Hill, A. F. Rigosi, and T. F. Heinz, Population inversion and giant bandgap renormalization in atomically thin WS2 layers, Nature Photonics **9**, 466 (2015).

[17] A. Steinhoff, M. Florian, M. Rösner, G. Schönhoff, T. O. Wehling, and F. Jahnke, Exciton fission in monolayer transition metal dichalcogenide semiconductors, Nature Communications **8**, 1166 (2017).

[18] T. Mueller and E. Malic, Exciton physics and device application of two-dimensional transition metal dichalcogenide semiconductors, npj 2D Materials and Applications **2**, 29 (2018).

[19] A. Arora, Magneto-optics of layered two-dimensional semiconductors and heterostructures: Progress and prospects, Journal of Applied Physics **129**, 120902 (2021).

[20] E. J. Sie, J. W. McIver, Y.-H. Lee, L. Fu, J. Kong, and N. Gedik, Valley-selective optical Stark effect in monolayer WS2, Nature Materials **14**, 290 (2015).

[21] E. Blundo, E. Cappelluti, M. Felici, G. Pettinari, and A. Polimeni, Strain-tuning of the electronic, optical, and vibrational properties of two-dimensional crystals, Applied Physics Reviews **8**, 021318 (2021).

[22] R. Rosati, K. Wagner, S. Brem, R. Perea-Causín, J. D. Ziegler, J. Zipfel, T. Taniguchi, K. Watanabe, A. Chernikov, and E. Malic, Non-equilibrium diffusion of dark excitons in atomically thin semiconductors, Nanoscale **13**, 19966 (2021).

[23] A. Raja, A. Chaves, J. Yu, G. Arefe, H. M. Hill, A. F. Rigosi, T. C. Berkelbach, P. Nagler, C. Schüller, T. Korn, C. Nuckolls, J. Hone, L. E. Brus, T. F. Heinz, D. R. Reichman, and A. Chernikov, Coulomb engineering of the bandgap and excitons in two-dimensional materials, Nature Communications **8**, 15251 (2017).

[24] S. Bertolazzi, M. Gobbi, Y. Zhao, C. Backes, and P. Samorì, Molecular chemistry approaches for tuning the properties of two-dimensional transition metal dichalcogenides, Chemical Society Reviews **47**, 6845 (2018).

[25] E. Lifshitz and L. Bykov, Microwave modulated and thermal modulated photoluminescence studies of 2H-lead iodide, The Journal of Physical Chemistry **97**, 9288 (1993).

[26] Z. Chen-Esterlit, E. Lifshitz, E. Cohen, and L. N. Pfeiffer, Microwave modulation of circularly polarized exciton photonluminescence in GaAs/AlAs multiple quantum wells, Physical Review B **53**, 10921 (1996).

[27] R. Guliamov, E. Lifshitz, E. Cohen, A. Ron, and H. Shtrikman, A Study of Semiconductor Quantum Structures by Microwave Modulated Photolumenescence, MRS Proceedings **573**, 119 (1999).

[28] I. Y. S. Ganichev, A. Dmitriev, S. Emel'yanov, Y. Terent'ev, I. Yaroshetskii, Impact ionization in a semiconductor in a light wave, JETP Lett **40**, 948 (1984).

[29] S. Zybell, H. Schneider, S. Winnerl, M. Wagner, K. Köhler, and M. Helm, Photoluminescence dynamics in GaAs/AlGaAs quantum wells under pulsed intersubband excitation, Applied Physics Letters **99**, 10.1063/1.3615298 (2011).

[30] W. Rice, J. Kono, S. Zybell, S. Winnerl, J. Bhattacharyya, H. Schneider, M. Helm, B. Ewers, A. Chernikov, M. Koch, S. Chatterjee, G. Khitrova, H. Gibbs, L. Schneebeli, B. Breddermann, M. Kira, and S. Koch, Observation of Forbidden Exciton Transitions Mediated by Coulomb Interactions in Photoexcited Semiconductor Quantum Wells, Physical Review Letters **110**, 137404 (2013).

[31] S. Leinß, T. Kampfrath, K. V.Volkmann, M. Wolf, J. T. Steiner, M. Kira, S. W. Koch, A. Leitenstorfer, and R. Huber, Terahertz Coherent Control of Optically Dark Paraexcitons in Cu_2O, Physical Review Letters **101**, 246401 (2008).

[32] C. Poellmann, P. Steinleitner, U. Leierseder, P. Nagler, G. Plechinger, M. Porer, R. Bratschitsch, C. Schüller, T. Korn, and R. Huber, Resonant internal quantum transitions and femtosecond radiative decay of excitons in monolayer WSe2, Nature Materials **14**, 889 (2015).

[33] E. J. Sie, C. H. Lui, Y.-H. Lee, L. Fu, J. Kong, and N. Gedik, Large, valley-exclusive Bloch-Siegert shift in monolayer WS 2, Science **355**, 1066 (2017).

[34] F. Langer, C. P. Schmid, S. Schlauderer, M. Gmitra, J. Fabian, P. Nagler, C. Schüller, T. Korn, P. G. Hawkins, J. T. Steiner, U. Huttner, S. W. Koch, M. Kira, and R. Huber, Lightwave valleytronics in a monolayer of tungsten diselenide, Nature **557**, 76 (2018).

[35] C.-K. Yong, M. I. B. Utama, C. S. Ong, T. Cao, E. C. Regan, J. Horng, Y. Shen, H. Cai, K. Watanabe, T. Taniguchi, S. Tongay, H. Deng, A. Zettl, S. G. Louie, and F. Wang, Valley-dependent exciton fine structure and AutlerTownes doublets from Berry phases in monolayer $MoSe_2$, Nature Materials **18**, 1065 (2019).

[36] T. Venanzi, M. Selig, S. Winnerl, A. Pashkin, A. Knorr, M. Helm, and H. Schneider, Terahertz-Induced Energy Transfer from Hot Carriers to Trions in a MoSe 2 Monolayer, ACS Photonics , acsphotonics.1c00394 (2021).

[37] T. Venanzi, M. Cuccu, R. Perea-Causin, X. Sun, S. Brem, D. Erkensten, T. Taniguchi, K. Watanabe, E. Malic, M. Helm, S. Winnerl, and A. Chernikov, Ultrafast switching of trions in 2D materials by terahertz photons, Nature Photonics **18**, 1344 (2024).

[38] O. Benson, C. Santori, M. Pelton, and Y. Yamamoto, Regulated and Entangled Photons from a Single Quantum Dot, Physical Review Letters **84**, 2513 (2000).

[39] Y.-M. He, O. Iff, N. Lundt, V. Baumann, M. Davanco, K. Srinivasan, S. Höfling, and C. Schneider, Cascaded emission of single photons from the biexciton in monolayered WSe2, Nature Communications **7**, 13409 (2016).

[40] A. Raja, L. Waldecker, J. Zipfel, Y. Cho, S. Brem, J. D. Ziegler, M. Kulig, T. Taniguchi, K. Watanabe, E. Malic, T. F. Heinz, T. C. Berkelbach, and A. Chernikov, Dielectric disorder in two-dimensional materials, Nature Nanotechnology **14**, 832 (2019).

[41] D. Rhodes, S. H. Chae, R. Ribeiro-Palau, and J. Hone, Disorder in van der Waals heterostructures of 2D materials, Nature Materials **18**, 541 (2019).

[42] A. Castellanos-Gomez, L. Vicarelli, E. Prada, J. O. Island, K. L. Narasimha-Acharya, S. I. Blanter, D. J. Groenendijk, M. Buscema, G. a. Steele, J. V. Alvarez, H. W. Zandbergen, J. J. Palacios, and H. S. J. van der Zant, Isolation and characterization of few-layer black phosphorus, 2D Materials **1**, 025001 (2014).

[43] M. Helm, S. Winnerl, A. Pashkin, J. M. Klopf, J.-C. Deinert, S. Kovalev, P. Evtushenko, U. Lehnert, R. Xiang, A. Arnold, A. Wagner, S. M. Schmidt, U. Schramm, T. Cowan, and P. Michel, The ELBE infrared and THz facility at Helmholtz-Zentrum Dresden-Rossendorf, The European Physical Journal Plus **138**, 158 (2023).

[44] Z. Li, T. Wang, C. Jin, Z. Lu, Z. Lian, Y. Meng, M. Blei, S. Gao, T. Taniguchi, K. Watanabe, T. Ren, S. Tongay, L. Yang, D. Smirnov, T. Cao, and S.-F. Shi, Emerging photoluminescence from the dark-exciton phonon replica in monolayer WSe2, Nature Communications **10**, 2469 (2019).

[45] M. He, P. Rivera, D. Van Tuan, N. P. Wilson, M. Yang, T. Taniguchi, K. Watanabe, J. Yan, D. G. Mandrus, H. Yu, H. Dery, W. Yao, and X. Xu, Valley phonons and exciton complexes in a monolayer semiconductor, Nature Communications **11**, 618 (2020).

[46] M. Yang, L. Ren, C. Robert, D. Van Tuan, L. Lombez, B. Urbaszek, X. Marie, and H. Dery, Relaxation and darkening of excitonic complexes in electrostatically doped monolayer WSe2: Roles of exciton-electron and trion-electron interactions, Physical Review B **105**, 085302 (2022).

[47] M. Selig, G. Berghäuser, M. Richter, R. Bratschitsch, A. Knorr, and E. Malic, Dark and bright exciton formation, thermalization, and photoluminescence in monolayer transition metal dichalcogenides, 2D Materials **5**, 035017 (2018).

[48] C. Robert, R. Picard, D. Lagarde, G. Wang, J. P. Echeverry, F. Cadiz, P. Renucci, A. Högele, T. Amand, X. Marie, I. C. Gerber, and B. Urbaszek, Excitonic properties of semiconducting monolayer and bilayer MoTe2, Physical Review B **94**, 155425 (2016).

[49] J. Zipfel, K. Wagner, M. A. Semina, J. D. Ziegler, T. Taniguchi, K. Watanabe, M. M. Glazov, and A. Chernikov, Electron recoil effect in electrically tunable MoSe2 monolayers, Physical Review B **105**, 075311 (2022).

[50] E. Courtade, M. Semina, M. Manca, M. M. Glazov, C. Robert, F. Cadiz, G. Wang, T. Taniguchi, K. Watanabe, M. Pierre, W. Escoffier, E. L. Ivchenko, P. Renucci, X. Marie, T. Amand, and B. Urbaszek, Charged excitons in monolayer WSe2 : Experiment and theory, Physical Review B **96**, 085302 (2017), arXiv:1705.02110.

[51] J. Zipfel, K. Wagner, J. D. Ziegler, T. Taniguchi, K. Watanabe, M. A. Semina, and A. Chernikov, Lightmatter coupling and non-equilibrium dynamics of exchange-split trions in monolayer WS2, The Journal of Chemical Physics **153**, 10.1063/5.0012721 (2020).

[52] N. A. Cordero, N. H. March, and J. A. Alonso, Ionization potentials of neutral atoms and positive ions in the limit of large atomic number, Physical Review A **75**, 012505 (2007).

[53] B. Jordon-Thaden, H. Kreckel, R. Golser, D. Schwalm, M. H. Berg, H. Buhr, H. Gnaser, M. Grieser, O. Heber, M. Lange, O. Novotný, S. Novotny, H. B. Pedersen, A. Petrignani, R. Repnow, H. Rubinstein, D. Shafir, A. Wolf, and D. Zajfman, Structure and Stability of the Negative Hydrogen Molecular Ion, Physical Review Letters **107**, 193003 (2011).

[54] P. Nagler, M. V. Ballottin, A. A. Mitioglu, M. V. Durnev, T. Taniguchi, K. Watanabe, A. Chernikov, C. Schüller, M. M. Glazov, P. C. M. Christianen, and T. Korn, Zeeman Splitting and Inverted Polarization of Biexciton Emission in Monolayer WS2, Physical Review Letters **121**, 057402 (2018).

[55] L. V. Keldysh, Ionization in the field of a strong electromagnetic wave, J. Exptl. Theoret. Phys. **20**, 56 (1965).

[56] T. Venanzi, M. Selig, A. Pashkin, S. Winnerl, M. Katzer, H. Arora, A. Erbe, A. Patanè, Z. R. Kudrynskyi, Z. D. Kovalyuk, L. Baldassarre, A. Knorr, M. Helm, and H. Schneider, Terahertz control of photoluminescence emission in few-layer InSe, Applied Physics Letters **120**, 092104 (2022).

[57] R. Rosati, K. Wagner, S. Brem, R. Perea-Causín, E. Wietek, J. Zipfel, J. D. Ziegler, M. Selig, T. Taniguchi, K. Watanabe, A. Knorr, A. Chernikov, and E. Malic, Temporal Evolution of Low-Temperature Phonon Sidebands in Transition Metal Dichalcogenides, ACS Photonics **7**, 2756 (2020).

[58] H. H. Fang, B. Han, C. Robert, M. A. Semina, D. Lagarde, E. Courtade, T. Taniguchi, K. Watanabe, T. Amand, B. Urbaszek, M. M. Glazov, and X. Marie, Control of the Exciton Radiative Lifetime in van der Waals Heterostructures, Physical Review Letters **123**, 067401 (2019).

[59] M. Selig, G. Berghäuser, A. Raja, P. Nagler, C. Schüller, T. F. Heinz, T. Korn, A. Chernikov, E. Malic, and A. Knorr, Excitonic linewidth and coherence lifetime in monolayer transition metal dichalcogenides, Nature Communications **7**, 13279 (2016).